
**H2020-MSCA-IF-2020**

**Secure Indoor Communication empowered by Intelligent reflecting Surface (SICIS)**

# D3.2

# Report on optimising IRS-aided indoor communication networks systematically

| | |
|---|---|
| **Authors(s)** | Sai Xu, Zeyang Li, Jie Zhang |
| **Author(s) Affiliation** | University of Sheffield, UK;<br>University of Sheffield, UK;<br>University of Sheffield, UK |
| **Editor(s)**: | Sai Xu |
| **Status-Version**: | V1.0 |
| **Project Number**: | 101032170 |
| **Project Title**: | Secure Indoor Communication empowered by Intelligent reflecting Surface |
| **Project Acronym:** | SICIS |
| **Work Package Number** | 3 |

## Abstract

Reconfigurable intelligent surface (RIS), which provides indirect line-of-sight (LoS) transmission paths between the receiver and its blocked transmitter, has been proposed as one of the promising technologies for network performance enhancement. Recent works indicate that both the numbers of RISs and unit cells per RIS have a significant impact on network performance. However, with a given total number of unit cells, the joint analysis of these two factors considering blockage effect has not been investigated. In this report, the coverage probability of a three-dimensional downlink millimeter wave RIS-assisted network is analyzed. We first derive the acceptable area where a LoS RIS is capable to satisfy the signal-to-noise ratio threshold at the receiver. Next, we model the centers of building blockages and human-body blockages as two independent Poisson point processes and derive the probability that indirect LoS transmissions exist. Then, we derive and validate the analytical upper and lower bounds of the coverage probability as the functions of network parameters and blockage densities. We also derive and validate the closed-form coverage probability when RISs are much closer to UE than BS. Finally, we propose a general network cost model for RIS-assisted network. Results show that in terms of coverage enhancement, densely deployed small-scale RISs outperform sparsely deployed large-scale RISs in scenarios with dense blockages or short transmission distances, while sparsely deployed large-scale RISs are preferable in scenarios with sparse blockages or long transmission distances.

The results presented in this deliverable have addressed the requirement of Task 3.2 in the SICIS project.



**Keywords:** Reconfigurable intelligent surfaces, three dimension, mmWave networks, blockage effect, coverage probability.

# Table of Contents

# 1. Introduction

Wireless data traffic will grow by up to 1000 times in the next decade [1]. To satisfy the immense data traffic demand, promising technologies, e.g., massive multiple-input multiple-output (MIMO) and ultra-dense network (UDN), have been proposed. By deploying more base stations (BSs) and more active antennas, the network capacity can be enhanced significantly. However, the hardware cost and energy consumption also increase dramatically. Therefore, reconfigurable intelligent surfaces (RISs), which have the advantage of less energy consumption and lower cost, have emerged to enhance the network performance. The work in [2] showed that the RIS-assisted networks with the proper number of BSs can achieve the highest cost effectiveness for coverage enhancement.

A RIS is a planar surface consisting of a large number of low-cost integrated electronic circuits (unit cells). Each integrated electronic circuit can be controlled to alter the phase and amplitude of the incident signal, so that the signal can be reconfigured to achieve different purpose, e.g., received power enhancement and signal/interference cancellation [3],[4]. An important application of RISs is to provide indirect line-of-sight (LoS) transmission paths when the direct transmission between the BS and user equipment (UE) is blocked. This is extremely useful in the millimeter wave (mmWave) networks [5],[6]. Besides, RISs are easy and flexible to be installed on the existing objects in both indoor and outdoor environments, which can significantly reduce the deployment cost. With all these advantages, RISs have drawn increasingly attention from various research, such as beamforming design based on deep reinforcement learning [7],[8], and channel estimation [9].

The performance of RIS-assisted networks under various scenarios has been widely studied recently. The coverage probability and ergodic capacity of the RIS-assisted single-input single-output (SISO) network have been derived [10],[11],[12]. The results in [11] indicated that both the number of RISs and the number of unit cells have a significant impact on the outage probability and average sum rate. The RIS-assisted networks under spatial correlated Rayleigh fading channels have been investigated in [13] and [14] and closed-form coverage probabilities have been derived. The results in [13] demonstrated that increasing the number of RISs is more beneficial than increasing unit cells. Different from above works which only considered Rayleigh fading channels, the RIS-assisted networks considering Rician fading channels have been investigated in [15] and [16]. The results in [15] showed that increasing the number of unit cells can significantly improve the network performance. For the above works, the spatial locations of RISs are not considered, or only one RIS/a given number of RISs at fixed locations are considered, and the impact of random spatial locations of RISs on the network performance were ignored.

Stochastic geometry has proved a tractable mathematical tool to model the spatial distribution of wireless nodes [17], and has been used to analyze the performance of RIS-assisted networks in only a few works. The works in [18] and [19] have studied RIS-assisted single-cell network with randomly distributed RISs and compared with decode-and-forward relays. The spatial throughput of the network by averaging the transmission distances was provided in [18]and the results indicated that given the total number of unit cells for RISs, the networks with fewer RISs but more unit cells per RIS have higher spatial throughput than the networks with more RISs but fewer unit cells per RIS. Nonetheless, the works in both [18] and [19] have only considered the scenario that the distance between the UE and RIS is much shorter than the distance between the UE and BS, so that the distances from the BS to RIS and to UE can be assumed to be approximately equal, which is less accurate. Multi-cell networks assisted by randomly distributed RISs have been investigated in [20],[21],[22], and [23]. The work in [20] provided the approximations for the coverage of the RIS-assisted mmWave networks. However, only the interference direct from BSs was considered. In [21] and [22], the interference reflected by RISs has been analyzed. The results in [21] showed that RIS-

assisted networks can enhance network capacity and energy efficiency when the BSs are not densely deployed. Nevertheless, the interference reflected by the RISs will limit the network performance when the BS density is higher than the RIS density. The power distributions of the signal and interference reflected by RISs were derived in [22]. Moreover, with a given total deployment cost and individual costs, the results revealed the existence of an optimal ratio between the density of RIS and BS for achieving the highest network throughput. The approximations of the coverage probability, ergodic capacity and energy efficiency of the RIS-assisted networks were derived in [23]. The LoS probability of direct transmission was considered in the work. For the above works, LoS transmission has been assumed between the BS/UE and RIS. However, there is no guarantee that RIS-assisted transmission will always be LoS in practice. Therefore, the probability that the RIS-assisted transmission is blocked needs to be investigated.

Blockage models based on Boolean line segments have been employed in the performance analysis of RIS-assisted networks. The work in [24] presented the probability that a randomly distributed RIS can be employed for RIS-assisted transmission. With RISs deployed on a subset of the blockages, the performance of RIS-assisted networks considering blockage effect was analyzed in [25],[26], and [27]. In [25], with a given distance between the BS and the UE, the outage probabilities of the RIS-assisted networks under three different RIS association strategies, i.e., a random RIS, the closest RIS, and multiple random RISs, were provided based on numerical integrals. In [26], the work assumed that the locations of BSs follow a PPP and each BS has a associated UE which locates at a fixed distance. The SIR coverage probability considering the interference from both direct transmission and reflective transmission of other BSs was calculated based on numerical integrals. In [27], the probability distribution of the path loss between the UE and its serving BS was derived. However, the path loss model of the RIS-assisted transmission in [27] can only be applied when either the transmitter or the receiver or both of them is/are in the near field of RIS [28], which is very uncommon especially when the size of the RIS is not large enough as compared with the transmission distances.

Research has shown that both the number of RISs and the number of unit cells per RIS have a great impact on the network performance. However, the effect of blockages on the RIS-assisted transmission, which plays an important role in the performance of mmWave RIS-assisted networks [29],[30], has been ignored in most of the above works. Only the work in [27] considered the blockage probability of the RIS-assisted transmission, but the path loss model can only apply to limited scenario. With a given total number of unit cells, the joint analysis of the RIS number and RIS size under various scenarios, e.g., different blockage density, transmission distance and received signal power requirement, has never been investigated so far. More specifically, whether fewer large RISs or more small RISs should be deployed for better network performance, and how to find the optimal number of unit cells per RIS still need to be studied with consideration of randomly distributed blockages.

Therefore, in this report, we investigate the RIS-assisted mmWave networks considering random blockages. Our main contributions are summarized as follows.

- We propose the earliest joint analysis on the impact of the RIS number and RIS size on the coverage probability considering blockage models. We consider both building blockage model and human-body blockage model. Meanwhile, we adopt Poisson point process (PPP) for the RIS distribution and blockage models. We present the three-dimensional (3D) communication model by considering the height of the blockages and wireless devices. In addition, we introduce the RIS size and density factor to determine the number of RISs and

the number of unit cells per RIS, so that different RIS deployment strategies can be evaluated and compared.

- We derive the analytical upper bound and lower bound of the coverage probability considering the network parameters and blockage densities, and derive the closed-form coverage probability when the connected RIS is much closer to the UE than the BS. Meanwhile, we provide the simulation results to validate our analytical results. In addition, we present a general cost model for RIS-assisted network.
- We analyze the effect of building density, nearby-user density, SNR threshold, the RIS size and RIS density on the coverage probability, respectively. We observe that more small RISs are better option for high building blockage density and/or short transmission distance, e.g., urban area, whereas fewer large RISs is more suitable for low building blockage density and/or long transmission distance, e.g., rural area. In addition, more small RISs is more applicable for small-cell networks and high human density, e.g., malls and airports. On the other hand, fewer large RISs is a better choice for the networks with high SNR requirement.

# 2. System Model and Problem Formulation

In this section, we present the system model of the RIS-assisted single-cell mmWave downlink networks. We first provide network model. Next, we describe blockage models, i.e., human-body blockage model and building blockage model. Finally, we describe the path loss model of both direct LoS transmission from the BS to the UE and indirect RIS-assisted transmission.

## 2.1. Network Model

The 3D RIS-assisted single-cell mmWave downlink networks are investigated. The BS has $N_t$ antennas and the UE has a single antenna. RISs are assumed to be distributed according to a PPP with density $\lambda_r$, as shown in Fig. 1. The horizontal distance between the BS and the UE, the BS and the $k_{th}$ RIS, the UE and the $k_{th}$ RIS is $R_b$, $l_k$ and $r_k$, respectively. In addition, the horizontal angle between the BS and the $k_{th}$ RIS at the UE is $\beta_k$. We assume that all the RISs have the same height $h_r$ and the angles of all the RISs are suitable for transmission[19],[21],[22]. Meanwhile, the height of the BS and UE is $h_b$ and $h_u$, as shown in Fig. 2.

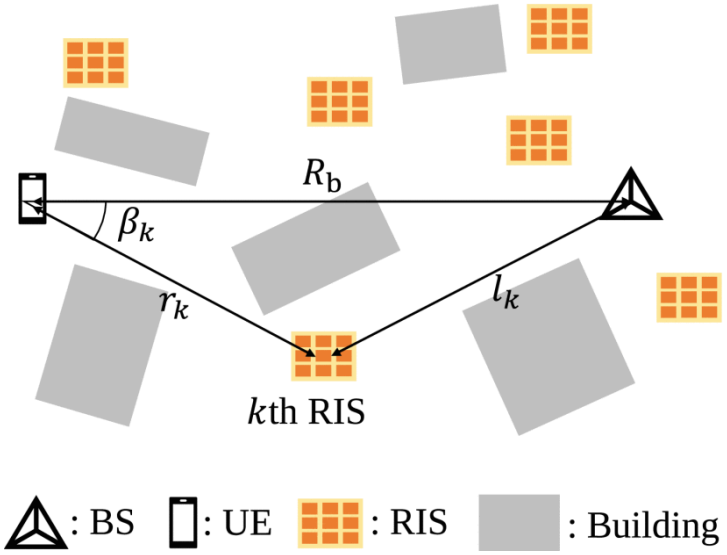


Fig. 1. Network model.

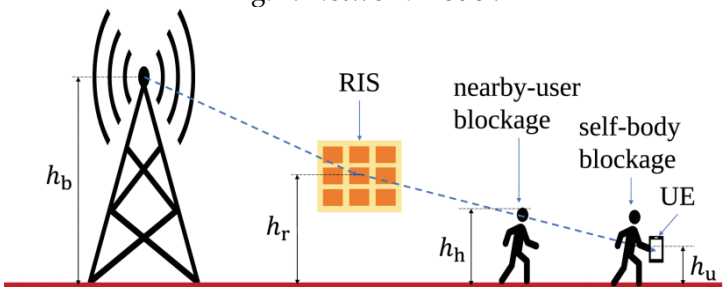


Fig. 2. Human-body blockages.

*Remark 1:* To investigate that whether large RISs with low density or small RISs with high density have higher network performance, first, we assume that the largest permitted RIS is made of $N \times M$ regularly arranged unit cells, where $N$ and $M$ represent the number of rows and columns of the unit cells for each RIS. Hence, the total number of unit cells per largest permitted RIS is $m_c = NM$. And

the width of each unit cell along both the x axis and y axis is $l_u$. In addition, the density of the largest permitted RISs is denoted by $\lambda_r'$. Then, we define the RIS size and density factor $n$, so that the largest permitted RIS is divided into $n$ small RISs. Nd and Md denote the number of rows and columns of the unit cells per RIS. Moreover, the total number of unit cells per RIS is $m_d = N_d M_d = \lfloor m_c / n \rfloor$ and $N_d / M_d \approx N / M$. Meanwhile, the density of divided RISs is denoted by $\lambda_r = n\lambda_r'$.n determines both the size of each RIS and the RIS density, thus it is a significant parameter to evaluate the network performance of different RIS deployment strategies.

## 2.2. Human-Body Blockage Model

As shown in Fig. 2, two types of human-body blockages are investigated: nearby-user blockages and self-body blockage. The 3D nearby-user blockage model and 3D self-body blockage model are shown in Fig. 3 and Fig. 4, respectively.

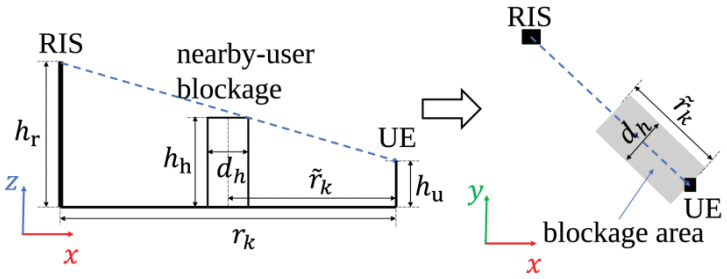


Fig. 3. Nearby-user blockage model.

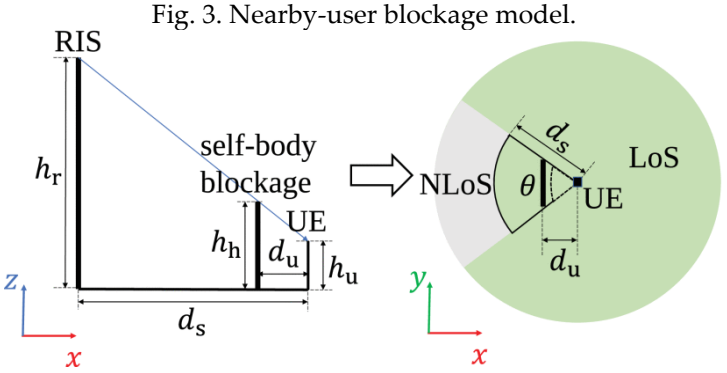


Fig. 4. Self-body blockage model.

For nearby-user blockage model, each blockage is modeled as a cylinder with diameter $d_h$ and height $h_h$. The centers of the cylinders are distributed according to a 2D homogeneous PPP with intensity $\lambda_h$. Due to the limited height of the nearby-user blockages, given the horizontal distance $r_k$ between the $k_{th}$ RIS and the UE, the horizontal distance of the transmission which can be blocked by nearby-user blockages is $r_k = \frac{h_h - h_u}{h_r - h_u} r_k$. Moreover, the transmission is blocked when the center of a blockage is located in the blockage area with size $d_h \times r_k$, as shown in Fig. 3. In PPP, the number of points in a certain area with size $S$ follows Poisson distribution with mean value $\lambda_h S$. Therefore, the probability that the transmission from the $k_{th}$ RIS to the UE is not blocked by nearby-user blockages is:

$$p_{\mathrm{nu}}(r_k) = e^{-\lambda_{\mathrm{h}} d_{\mathrm{h}} \frac{h_{\mathrm{h}} - h_{\mathrm{u}}}{h_{\mathrm{r}} - h_{\mathrm{u}}} r_k}.$$

Besides, we assume that both the BS and RISs are higher than nearby-user blockages. Therefore, the transmission between the BS and the RIS cannot be blocked by nearby-user blockages.

For self-body blockage model, since the height $h_{\mathrm{h}}$ of the blockage is limited, the transmission cannot be blocked by self-body blockage if the horizontal distance between the RIS and the UE is less than $d_{\mathrm{s}} = \frac{h_{\mathrm{r}} - h_{\mathrm{u}}}{h_{\mathrm{h}} - h_{\mathrm{u}}} d_{\mathrm{u}}$, where $d_{\mathrm{u}}$ is the horizontal distance between the UE and the user, as shown in Fig. 4. On the other hand, when the horizontal distance between the UE and the RIS is larger than $d_{\mathrm{s}}$, the angle of the self-body blockage at the UE is $\theta$. Moreover, the probability that the transmission from the $k_{th}$ RIS to the UE is not blocked by self-body blockage is:

$$p_{\mathrm{su}}(r_k) = \begin{cases} 1, & r_k \le d_{\mathrm{s}}, \\ 1 - \frac{\theta}{2\pi}, & \text{otherwise.} \end{cases}$$

## 2.3. Building Blockage Model

The blockages caused by buildings and permanent structures are modeled using random shape theory. All the building blockages are assumed to be rectangles. The centers of the blockages are distributed according to a PPP with intensity $\lambda_{\mathrm{b}}$. The lengths and widths of the building blockages are assumed to follow two independent distributions with the expected length $L$ and the expected width $W$, respectively. Meanwhile, the orientation of the building blockages follows uniform distribution in $(0, 2\pi]$. Furthermore, the probability that the transmission from the $k_{th}$ RIS to the UE is not blocked by building blockages is [31]:

$$p_{\mathrm{bu}}(r_k) = e^{-\psi r_k - \varpi},$$

where $\psi = 2\lambda_{\mathrm{b}}(W + L)/\pi$ and $\varpi = \lambda_{\mathrm{b}} LW$. Since all the RISs are pre-deployed, no building blockage is located between the BS and the RISs. Therefore, the transmissions between the BS and the RISs always be LoS.

## 2.4. Received Signal Power

Both the direct transmission from the BS to the UE and the RIS-assisted transmission are considered. The wavelength of the signal is denoted by $\mu$ and the path loss exponent is $\alpha$. Let $P_{\mathrm{t}}$ and $G_{\mathrm{t}}$ denote the transmit power and antenna gain of the BS. In this report, small-scale fading is omitted because 1) it is not significant in LoS mmWave transmission [21],[27],[30],[32],[33]; 2) the effect of channel hardening exits when the number of elements of antennas/RISs is sufficiently large [34],[35]. In addition, due to high penetration loss of mmWave frequency [36], non-line-of-sight (NLoS) transmission is not considere. Furthermore, the received signal power of the direct LoS transmission from the BS to the UE is as follows:

$$P_{\mathrm{rb}} = \frac{P_{\mathrm{t}} N_{\mathrm{t}}^2 G_{\mathrm{t}} \mu^2}{16\pi^2 (R_{\mathrm{b}}^2 + (h_{\mathrm{b}} - h_{\mathrm{u}})^2)^{\frac{\alpha}{2}}}.$$

RIS-assisted transmission is adopted when the direct transmission is blocked. For RIS-assisted transmission, the power radiation pattern of RISs is assumed to be independent of the incident/reflected angle of the signal and the peak radiation is considered in all the directions. All the unit cells of the RIS have the same amplitude $\rho$ of the reflection coefficient and implement perfect phase control, so that the reflected signals from the unit cells are aligned in phase at the receiver to enhance the received signal power. Therefore, the received signal power of the RIS-assisted transmission can be formulated as follows [28]:

$$P_{\mathrm{rr}} = \frac{P_{\mathrm{t}} N_{\mathrm{t}}^2 G_{\mathrm{t}} M_{\mathrm{d}}^2 N_{\mathrm{d}}^2 l_{\mathrm{u}}^2 \mu^2 \rho^2}{64\pi^3 (l_k r_k)^{\alpha}},$$

where $l_k = (l_k^2 + (h_{\mathrm{b}} - h_{\mathrm{r}})^2)^{\frac{1}{2}}$ is the transmission distance between the BS and the $k_{th}$ RIS, $l_k = (R_{\mathrm{b}}^2 + r_k^2 - 2R_{\mathrm{b}} r_k \cos\beta_k)^{\frac{1}{2}}$, $r_k = (r_k^2 + (h_{\mathrm{r}} - h_{\mathrm{u}})^2)^{\frac{1}{2}}$ is the transmission distance between the $k_{th}$ RIS and the UE, G denotes the channel gain of each RIS. Furthermore, the SNR of the received signal is computed by:

$$\mathrm{SNR} = \frac{P_{\mathrm{r}}}{w_0},$$

where $P_{\mathrm{r}}$ denotes the received signal power (depends on whether it is direct transmission from the BS to the UE or RIS-assisted transmission, $P_{\mathrm{r}} = P_{\mathrm{rb}}$ or $P_{\mathrm{rr}}$ ) and $w_0$ is the noise power.

# 3. Coverage Probability

In this section, we derive the analytical upper and lower bounds of the coverage probability. A UE is in coverage when two conditions are met: 1) the SNR of the received signal is higher than the SNR threshold $T$ ; 2) either the direct transmission from the BS to the UE or the RIS-assisted transmission is unblocked. Note that these two conditions are independent from each other, i.e., the received SNR in condition 1) is calculated without considering any penetration loss. Meanwhile, condition 2) does not imply condition 1) because even though the transmission is unblocked, it is possible that the SNR of the received signal is below the SNR threshold. We analyze these two conditions in the following two subsections, respectively. Moreover, we present the analytical expressions of the lower bound and upper bound of the coverage probability in the end of this section.

## 3.1. The RIS-Assisted Transmission With Acceptable SNR

The SNR of the RIS-assisted transmission is determined by the transmission distance between the BS and the RIS and between the UE and the RIS. Therefore, given the distance between the BS and the UE, a RIS can only be located in a certain area to satisfy the SNR threshold, and this area is named the RIS are. The RIS area depends on various factors, e.g., the size of RISs, transmission distance and SNR threshold. Based on the inequation $P_{\mathrm{rr}} / w_0 \geq T$ , the mathematical expression of the RIS area is provided in the following proposition1:

*Proposition 1:* For the RIS-assisted transmission, given the SNR threshold $T$ , the RIS area can be formulated as:

$$\{(r\cos\beta, r\sin\beta) \mid r \geq 0, \beta \in (0, 2\pi],$$
$$r^4 + br^3\cos\beta + cr^2 + dr\cos\beta + u \geq 0\},$$

where $r$ is the horizontal distance between the RIS and the UE, $\beta$ is the horizontal angle between the BS and the RIS at the UE, $b = -2R_{\mathrm{b}}$ , $c = R_{\mathrm{b}}^2 + (h_{\mathrm{b}} - h_{\mathrm{r}})^2 + (h_{\mathrm{r}} - h_{\mathrm{u}})^2$ , $d = -2(h_{\mathrm{r}} - h_{\mathrm{u}})^2 R_{\mathrm{b}}$ , $u = R_{\mathrm{b}}^2(h_{\mathrm{r}} - h_{\mathrm{u}})^2 + (h_{\mathrm{r}} - h_{\mathrm{u}})^2(h_{\mathrm{b}} - h_{\mathrm{r}})^2 - \left( \frac{P_{\mathrm{t}} N_{\mathrm{t}}^2 G_{\mathrm{t}} M_{\mathrm{d}}^2 N_{\mathrm{d}}^2 l_{\mathrm{u}}^2 \mu^2 \rho^2}{64\pi^3 w_0 T} \right)^{\frac{2}{\alpha}}$ .

The SNR of the received signal when the RIS is located at $(x, y)$ is shown in Fig. 5, where the locations of the UE and the BS are $(0,0)$ and $(150,0)$ , respectively. With a given SNR threshold. With different SNR threshold $T$ , the RIS area is a various irregular graphic, which is very difficult to be adopted for the network coverage analysis. Therefore, for the simplicity of analysis, circle/circles centered on the UE and BS are adopted to represent the upper/lower bounds of the RIS area. The principles of drawing the RIS area upper/lower bounds are: 1) the centers of the circles for the upper and lower bounds must be the UE or BS; 2) for lower bound, the circle/circles must be contained in the RIS area and cannot be overlapped with each other if there are two circles; 3) for upper bound, the circle/circles need to be large enough to cover all the RIS area. Based on these principles, the

shapes of the RIS area are classified into four typical scenarios. As the SNR threshold $T$ increases, the four typical scenarios are shown as the grey area in Fig. 5–8:

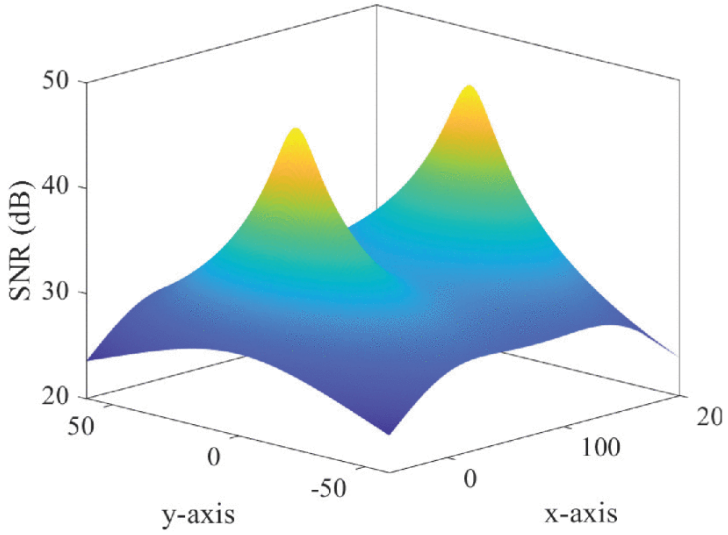


Fig. 5. The SNR of the received signal when the RIS is located at $(x, y)$. The locations of the UE and the BS are $(0,0)$ and $(150,0)$, respectively.

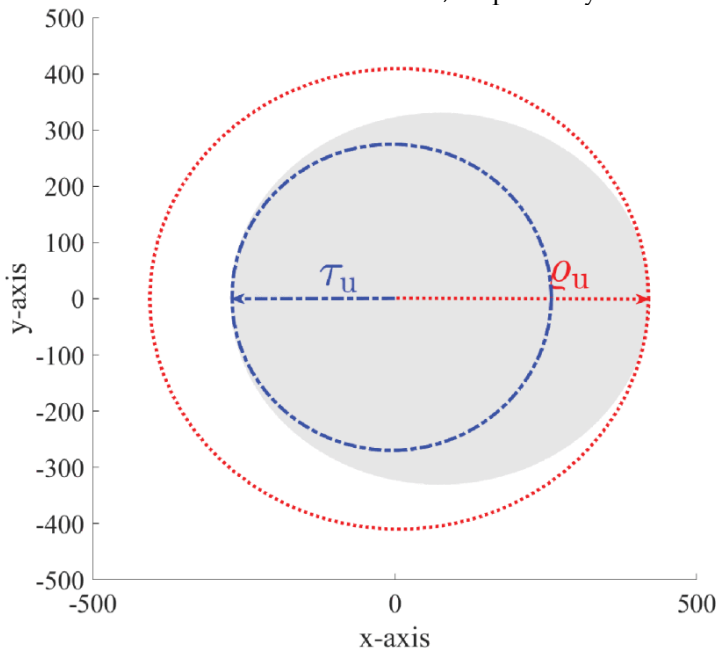


Fig. 6. The RIS area when the SNR threshold T=18dB.

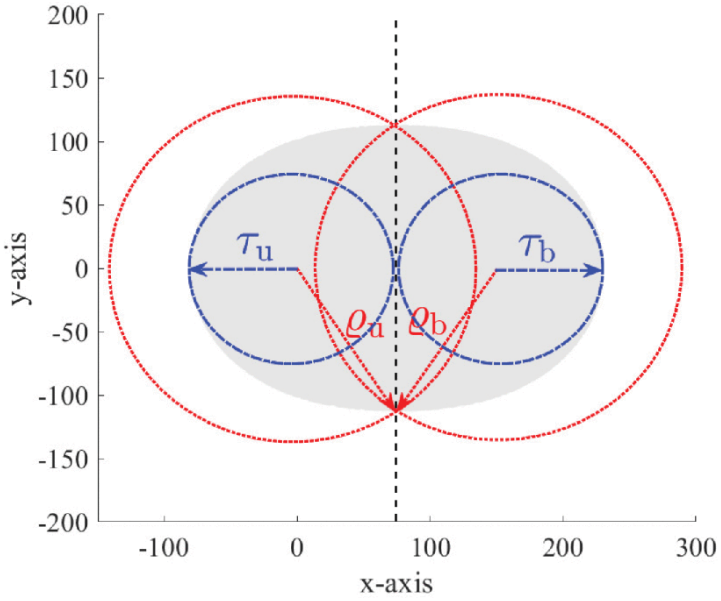


Fig. 7. The RIS area when the SNR threshold T=23dB.

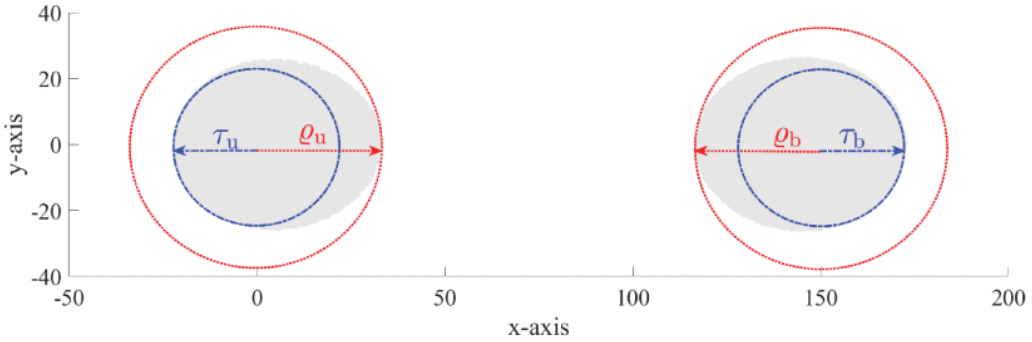


Fig. 8. The RIS area when the SNR threshold T=36dB.

**Table I** $\tau_u, \tau_b, \tilde{n}_u$ and $\tilde{n}_u$ when $\Delta = 0, AB > 0, C \neq 0$

| Case | Condition | $\varrho_u \vee (\varrho_{u1}, \varrho_{u2})$ | $\varrho_b \vee (\varrho_{b1}, \varrho_{b2})$ | $\tau_b$ | $\tau_u$ |
|---|---|---|---|---|---|
| 1 | $x_1 < 0$ | $\varrho_u = x_2$ | $\varrho_b = 0$ | 0 | $\lvert x_1 \rvert$ |
| 2 | $x_1 \geq 0, x_2 < R_b/2$ | $\varrho_{u1} = x_1, \varrho_{u2} = x_2$ | $\varrho_b = 0$ | 0 | 0 |
| 3 | $x_1 \geq R_b/2, x_2 < R_b$ | $\varrho_u = 0$ | $\varrho_{b1} = R_b - x_2, \varrho_{b2} = R_b - x_1$ | 0 | 0 |
| 4 | $x_2 \geq R_b$ | $\varrho_u = 0$ | $\varrho_b = R_b - x_1$ | $x_2 - R_b$ | 0 |

**Table II** $\tau_u, \tau_b, \tilde{n}_u$ and $\tilde{n}_u$ when $\Delta > 0,\ x_1 < 0,\ x_2 < R_b$

| Case | Condition | | $\varrho_u$ | $\varrho_b$ | $\tau_b$ | $\tau_u$ |
|---|---|---|---|---|---|---|
| 1 | $\lvert x_1 \rvert \geq R_b$ | | $x_2$ | 0 | 0 | $\lvert x_1 \rvert$ |
| 2 | $\lvert x_1 \rvert < R_b$ | $\lvert x_1 \rvert + x_2 \geq 2R_b$ | $\sqrt{\frac{-\sigma+\sqrt{\sigma^2-4\chi}}{2} + \frac{R_b^2}{4}}$ | | $x_2 - R_b$ | |
| | | $\lvert x_1 \rvert + x_2 < 2R_b$ | | | $R_b - \lvert x_1 \rvert$ | |

**Table III** $\tau_u, \tau_b, \tilde{n}_u$ and $\tilde{n}_u$ when $\Delta > 0,\ x_1 < 0,\ x_2 > R_b$

| Case | Condition | $\varrho_u \vee (\varrho_{u1}, \varrho_{u2})$ | $\varrho_b \vee (\varrho_{b1}, \varrho_{b2})$ | $\tau_b$ | $\tau_u$ |
|---|---|---|---|---|---|
| 1 | $x_1 < 0, x_2 < R_b$ | $\varrho_u = x_2$ | $\varrho_b = 0$ | 0 | $\lvert x_1 \rvert$ |
| 2 | $x_1 \geq 0, x_2 < R_b/2$ | $\varrho_{u1} = x_1, \varrho_{u2} = x_2$ | $\varrho_b = 0$ | 0 | 0 |
| 3 | $x_1 \geq R_b/2, x_2 < R_b$ | $\varrho_u = 0$ | $\varrho_{b1} = R_b - x_2, \varrho_{b2} = R_b - x_1$ | 0 | 0 |
| 4 | $x_1 \geq 0, x_2 \geq R_b$ | $\varrho_u = 0$ | $\varrho_b = R_b - x_1$ | $x_2 - R_b$ | 0 |

## 3.2. The Probability for LoS Transmission

For RIS-assisted transmission, since the transmission between the BS and the RIS always be LoS, whether the RIS-assisted transmission is blocked or unblocked depends on whether or not any blockages are located between the RIS and the UE. Indirect LoS RIS-assisted transmission exists if no blockage is located between the RIS and the UE. The probability for LoS transmission with the horizontal distance $r$ is provided inLemma 2.

*Lemma 3:* Given the horizontal transmission distance $r$, the probability that the transmission is LoS is expressed by:

$$p_{\mathrm{u}}(r)=\begin{cases} e^{\upsilon r-\varpi}, & r\le d_{\mathrm{s}}, \\ \left(1-\dfrac{\theta}{2\pi}\right)e^{\upsilon r-\varpi}, & \text{otherwise.} \end{cases}$$

where $\upsilon=-d_{\mathrm{h}}\lambda_{\mathrm{h}}\dfrac{h_{\mathrm{h}}-h_{\mathrm{u}}}{h_{\mathrm{r}}-h_{\mathrm{u}}}-\psi$ When the transmission is from the RIS to the UE, and $\upsilon=-d_{\mathrm{h}}\lambda_{\mathrm{h}}\dfrac{h_{\mathrm{h}}-h_{\mathrm{u}}}{h_{\mathrm{b}}-h_{\mathrm{u}}}-\psi$ When the transmission is from the BS to the UE.

*Proof:*

$$p_{\mathrm{u}}(r)=p_{\mathrm{nu}}(r)p_{\mathrm{su}}(r)p_{\mathrm{bu}}(r)=\begin{cases} e^{\left(-d_{\mathrm{h}}\lambda_{\mathrm{h}}\frac{h_{\mathrm{h}}-h_{\mathrm{u}}}{h_{\mathrm{r}}-h_{\mathrm{u}}}-\psi\right)r-\varpi}, & r\le d_{\mathrm{s}}, \\ \left(1-\dfrac{\theta}{2\pi}\right)e^{\left(-d_{\mathrm{h}}\lambda_{\mathrm{h}}\frac{h_{\mathrm{h}}-h_{\mathrm{u}}}{h_{\mathrm{r}}-h_{\mathrm{u}}}-\psi\right)r-\varpi}, & \text{otherwise.} \end{cases}$$

Based on *Lemma 2*, when the RISs are randomly distributed within a circle or a circular ring, the probability that the indirect LoS RIS-assisted transmission exists is presented in Lemma 3.

*Lemma 4:* When RISs are randomly located within the circle centered on the UE with radius $R_{\mathrm{t}}$, the probability that the indirect LoS RIS-assisted transmission exists can be expressed as:

$$\Phi_{\mathrm{uc}}(R_{\mathrm{t}})=\begin{cases} 1-e^{\gamma_1\grave{\mathrm{o}}_1-\gamma_1}, & R_{\mathrm{t}}<d_{\mathrm{s}}, \\ e^{-\gamma_1}\left(e^{\gamma_1(\grave{\mathrm{o}}_2+\zeta_1)}-e^{\gamma_1(\eta_1+\kappa_1)}\right), & R_{\mathrm{t}}\ge d_{\mathrm{s}}, \end{cases}$$

where

$$\begin{cases}\gamma_1=\pi R_{\mathrm{t}}^2\lambda_{\mathrm{r}},\\ \dot{o}_1=1-\dfrac{2e^{-\varpi}\left(1+e^{\upsilon R_{\mathrm{t}}}(\upsilon R_{\mathrm{t}}-1)\right)}{\upsilon^2R_{\mathrm{t}}^2},\\ \dot{o}_2=\dfrac{d_{\mathrm{s}}^2}{R_{\mathrm{t}}^2},\\ \zeta_1=\dfrac{R_{\mathrm{t}}^2-d_{\mathrm{s}}^2}{R_{\mathrm{t}}^2},\\ \eta_1=\dfrac{d_{\mathrm{s}}^2}{R_{\mathrm{t}}^2}-\dfrac{2e^{-\varpi}\left(1+e^{\upsilon d_{\mathrm{s}}}(\upsilon d_{\mathrm{s}}-1)\right)}{\upsilon^2R_{\mathrm{t}}^2},\\ \begin{cases}\kappa_1=f_1(R_{\mathrm{t}},d_{\mathrm{s}})=\dfrac{R_{\mathrm{t}}^2-d_{\mathrm{s}}^2}{R_{\mathrm{t}}^2}\\ -\dfrac{2\left(1-\dfrac{\theta}{2\pi}\right)e^{-\varpi}\left(e^{\upsilon d_{\mathrm{s}}}(1-\upsilon d_{\mathrm{s}})+e^{\upsilon R_{\mathrm{t}}}(\upsilon R_{\mathrm{t}}-1)\right)}{\upsilon^2R_{\mathrm{t}}^2};\end{cases}\end{cases}$$

When the RISs are randomly located within the circle centered on the BS with radius $R_{\mathrm{t}}$ the probability that the indirect LoS RIS-assisted transmission exists can be expressed as

$$\Phi_{\mathrm{bc}}(R_{\mathrm{t}})=1-e^{\gamma_1\dot{o}_3-\gamma_1},$$

where

$$\begin{cases}\dot{o}_3=f_2(R_{\mathrm{t}},0),\\ \begin{cases}f_2(x,y)=\dfrac{x^2-y^2}{x^2}-\left(1-\dfrac{\theta}{2\pi}\right)\dfrac{2}{\pi x^2}\\ \int_0^{\pi}\int_0^{x}re^{\upsilon\sqrt{R_{\mathrm{b}}^2+r^2-2R_{\mathrm{b}}r\cos\beta}-\varpi}\mathrm{d}r\mathrm{d}\beta;\end{cases}\end{cases}$$

When RISs are randomly located within the circular ring centered on the UE with small radius $R_{\mathrm{t1}}$ and large radius $R_{\mathrm{t2}}$, the probability that indirect LoS RIS-assisted transmission exists is:

$$\Phi_{\mathrm{ur}}(R_{\mathrm{t1}},R_{\mathrm{t2}})=\begin{cases}e^{\gamma_2\dot{o}_4-\gamma_2}\left(e^{\gamma_2\zeta_2}-e^{\gamma_2\eta_2}\right), & R_{\mathrm{t1}}<R_{\mathrm{t2}}<d_{\mathrm{s}},\\ e^{\gamma_2\dot{o}_4-\gamma_2}\left(e^{\gamma_2(\xi_1+\zeta_3)}-e^{\gamma_2(\eta_3+\kappa_2)}\right), & R_{\mathrm{t1}}<d_{\mathrm{s}}\le R_{\mathrm{t2}},\\ e^{\gamma_2\dot{o}_4-\gamma_2}\left(e^{\gamma_2\zeta_2}-e^{\gamma_2\eta_4}\right), & d_{\mathrm{s}}\le R_{\mathrm{t1}}<R_{\mathrm{t2}},\end{cases}$$

where

$$\begin{cases} \gamma_2 = \pi R_{t2}^2 \lambda_r, \\ \grave{o}_4 = \dfrac{R_{t1}^2}{R_{t2}^2}, \\ \zeta_2 = \dfrac{R_{t2}^2 - R_{t1}^2}{R_{t2}^2}, \\ \begin{cases} \eta_2 = g(R_{t2}, R_{t1}) = \dfrac{R_{t2}^2 - R_{t1}^2}{R_{t2}^2} \\ -\dfrac{2e^{-\varpi}\left(e^{\upsilon R_{t1}}(1-\upsilon R_{t1}) + e^{\upsilon R_{t2}}(\upsilon R_{t2}-1)\right)}{\upsilon^2 R_{t2}^2}, \end{cases} \\ \xi_1 = \dfrac{d_s^2 - R_{t1}^2}{R_{t2}^2}, \\ \zeta_3 = \dfrac{R_{t2}^2 - d_s^2}{R_{t2}^2}, \\ \eta_3 = g(d_s, R_{t1}), \\ \kappa_2 = f_1(R_{t2}, d_s), \\ \eta_4 = f_1(R_{t2}, R_{t1}); \end{cases}$$

When the RISs are randomly located within the circular ring centered on the BS with the small radius $R_{t1}$ and the large radius $R_{t2}$, the probability that the indirect LoS RIS-assisted transmission exists is:

$$\Phi_{br}(R_{t1}, R_{t2}) = e^{\gamma_2 \grave{o}_4 - \gamma_2}\left(e^{\gamma_2 \zeta_2} - e^{\gamma_2 \eta_5}\right),$$

Where $\eta_5 = f_2(R_{t2}, R_{t1})$

## 3.3. Special Case: RISs are Much Closer to UE Than BS

In this subsection, we focus on a common scenario where the horizontal distance between the connected RIS and UE is much shorter than the horizontal distance between the BS and UE[18],[19],[22]. In this scenario, the horizontal distance between the BS and connected RIS can be approximated as the same as the horizontal distance between the BS and UE, i.e., $l_k \approx R_b$. With a given SNR threshold $T$, the radius $R_u$ of the RIS area can be derived from $P_{rr} / w_0 \geq T$, which is express by:

$$R_u = \sqrt{\frac{1}{R_b^2 + (h_b - h_r)^2}\left(\frac{Z}{Tw_0}\right)^{\frac{2}{\alpha}} - (h_r - h_u)^2},$$

where $Z = \dfrac{P_t N_t^2 G_t M_d^2 N_d^2 l_u^2 \mu^2 \rho^2}{64\pi^3}$. Note that outage happens if $\dfrac{1}{R_b^2 + (h_b - h_r)^2}\left(\dfrac{Z}{Tw_0}\right)^{\frac{2}{\alpha}} < (h_r - h_u)^2$.

Moreover, considering nearby-user blockages and building blockages, the coverage probability can be derived based onequation (10)inLemma 3, which is presented in the following lemma:

*Lemma 7:* When the horizontal distance between the connected RIS and UE is much shorter than the distance between the BS and UE, the closed-form coverage probability of the RIS-assisted network can be expressed inequation (20), shown at the bottom of the next page.

$$\Psi_{\mathrm{a}} = 1 - \exp\left( \pi R_{\mathrm{u}}^2 \lambda_{\mathrm{r}} \left( 1 - \frac{2e^{-\varpi}\left(1 + e^{\upsilon R_{\mathrm{u}}}(\upsilon R_{\mathrm{u}} - 1)\right)}{\upsilon^2 R_{\mathrm{u}}^2} \right) - \pi R_{\mathrm{u}}^2 \lambda_{\mathrm{r}} \right),$$

where $R_{\mathrm{u}}$ is decided by the SNR threshold $T$, $\upsilon = -d_{\mathrm{h}}\lambda_{\mathrm{h}} \frac{h_{\mathrm{h}} - h_{\mathrm{u}}}{h_{\mathrm{r}} - h_{\mathrm{u}}} - 2\lambda_{\mathrm{b}}(W + L)/\pi$ and $\varpi = \lambda_{\mathrm{b}} LW$ are decided by the size, height and density of the blockages, including nearby-user blockages and building blockages.

## 3.4. Cost Effectiveness

Even the total number of unit cells is the same, the cost of RIS implementation might be different with different number of RISs. Specifically, the costs of RIS implementation, land acquisition, channel estimation and signal processing might be increasing with the number of RISs. However, it is unclear whether the total cost linearly growth with the number of RISs or not, especially when the number of unit cells decreases as the number of RISs increases. Therefore, we propose a general model for the total cost of RIS implementation as a function of $n$ (as mentioned in system model, $n$ is the number of RISs divided from the total number of unit cells). The equation is presented as follows:

$$C_{\mathrm{ost}} = c_{\mathrm{ost}} n^{\varsigma},$$

where $c_{\mathrm{ost}}$ and $\varsigma$ are the cost indexes decided by the industry, particularly, $\varsigma$ is the exponent to indicate how the number of RISs affects the total cost, e.g., $\varsigma$ =1means that the total cost grows linearly with the number of RISs, while $\varsigma$ =0means that the total cost is fixed despite of the number of RISs.

# 4. Numerical Results

In this section, the coverage probability of RIS-assisted wireless networks is analyzed and the analytical results are validated via Monte Carlo simulations. As mentioned in the system model, the parameter decides both the RIS density and the RIS size. Under various scenarios, i.e., different building density, human density, transmission distance and SNR threshold, the optimal value of which leads to the highest coverage probability is different. The system parameters are shown in Table IV if not mentioned otherwise. Similar settings of simulation parameters can be found in [19],[28],[31],[37], and [38].

**TABLE IV**Simulation Parameters

| parameter | value | parameter | value |
|---|---|---|---|
| $M$ | 50 | $N$ | 50 |
| $N_{\mathrm{t}}$ | 128 | $h_{\mathrm{r}}$ | 15 m |
| $h_{\mathrm{b}}$ | 30 m | $h_{\mathrm{u}}$ | 1.3 m |
| $h_{\mathrm{h}}$ | 1.7 m | $d_{\mathrm{h}}$ | 0.4 m |
| $\lambda_{\mathrm{h}}$ | 0.3 $/\mathrm{m}^2$ | $d_{\mathrm{u}}$ | 0.1 m |
| $\theta$ | $\pi/3$ | $\lambda_{\mathrm{b}}$ | $2 \times 10^{-3}$ $/\mathrm{m}^2$ |
| $\lambda_{\mathrm{r}}'$ | $5 \times 10^{-4}$ $/\mathrm{m}^2$ | $L$ | 15 m |
| $W$ | 10 m | $\alpha$ | 2 |
| $\mu$ | 0.01 m | $P_{\mathrm{t}}$ | 1 W |
| $G_{\mathrm{t}}$ | 1 | $\rho$ | 0.9 |
| $l_{\mathrm{u}}$ | 0.005 m | $w_0$ | -90 dBm |
| $T$ | 20 dB | $R_{\mathrm{b}}$ | 250 m |

In Fig. 10, the coverage probabilities to the building blockage density are shown. In each subfigure, different distance between the BS and the UE is applied, and the comparison between different values of $n$ is demonstrated. Firstly, the analytical results are validated by showing that both lower bound and upper bound have the same trend as the simulation results. Secondly, it is indicated that the density of building blockages has less impact on the coverage probability with larger $n$ .Thirdly, as the distance between the BS and the UE rises, the coverage probability with larger $n$ decreases faster than the coverage probability with smaller $n$ . The reason is that larger $n$ means smaller size of RISs, which leads to lower received signal power gain and is more sensitive to the increase of transmission distance. For these reasons, when $R_{\mathrm{b}} = 50$ m, the RIS-assisted networks with $n = 3$ have the highest coverage probability. However, when $R_{\mathrm{b}} = 250$ m and $\lambda_{\mathrm{b}} \le 2.7 \times 10^{-3} / \mathrm{m}^2$ , the networks with $n = 2$ have the highest coverage; and when $R_{\mathrm{b}} = 250$ m and $\lambda_{\mathrm{b}} \le 2.7 \times 10^{-3} / \mathrm{m}^2$ , the RIS-assisted networks with $n = 3$ have the highest coverage probability. As a result, large $n$ is suitable for high building blockage density and/or short transmission distance, e.g., urban area, whereas small $n$ is more applicable for low building blockage density and/or long transmission distance, e.g., rural area. In addition, in the same cell of a BS, small-scale RISs are preferable to be deployed around the cell center, while large-scale RISs are preferable to be deployed in the cell edge.

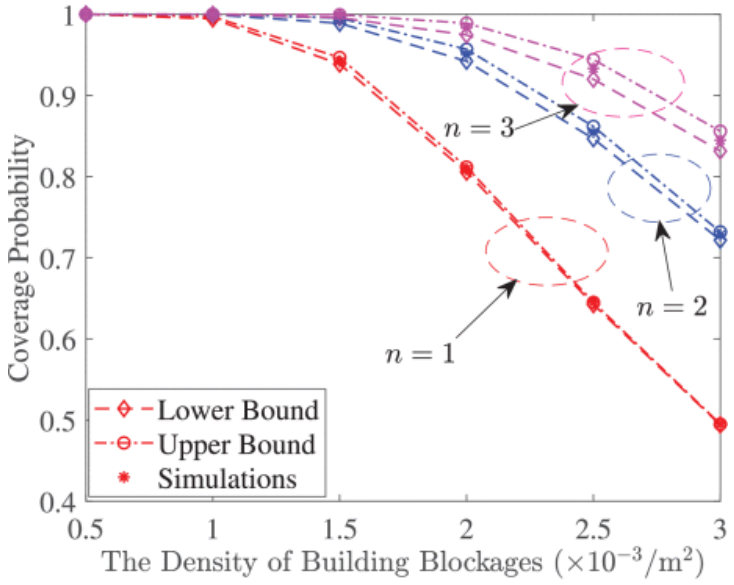


(a) $R_{\mathrm{b}} = 50$ m

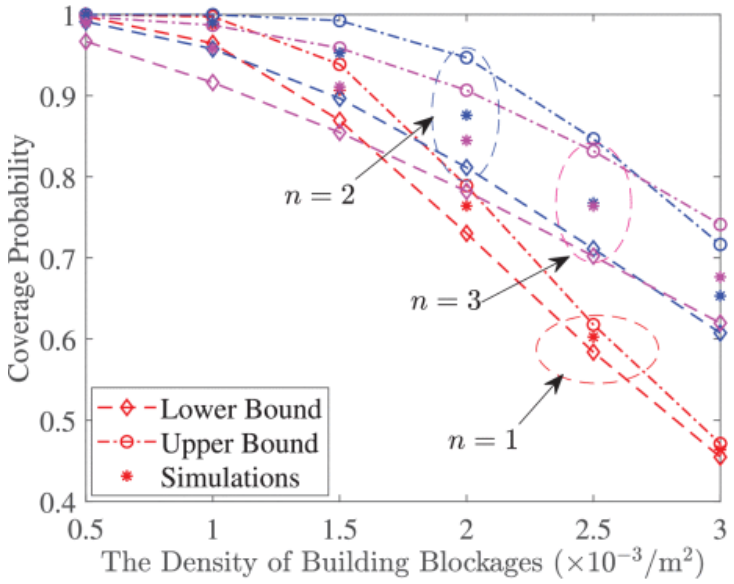


(b) $R_{\mathrm{b}} = 250$ m

Fig. 10. With different distance between the BS and the UE, the coverage probability to the density of building blockages.

Fig. 11shows the effect of the nearby-user blockages on the coverage probability.Fig. 11 (a)shows that when the horizontal transmission distance $R_{\mathrm{b}} = 50m$ , $n = 3$has the highest coverage. However, inFig. 11 (b), when the horizontal transmission distance increases to 250m, $n = 3$has the highest coverage, and as the nearby-user blockage density rises to 0.5 /m$^2$, $n = 2$and $n = 3$have almost the same coverage.Fig. 11indicates that the networks with larger $n$ are less sensitive to the increase of the nearby-user blockage density. In addition, increasing $n$ can be more beneficial for the case with high nearby-user density. Consequently, large $n$ is more applicable for the places which deploy small-cell networks and have high human density, e.g., malls and airports.

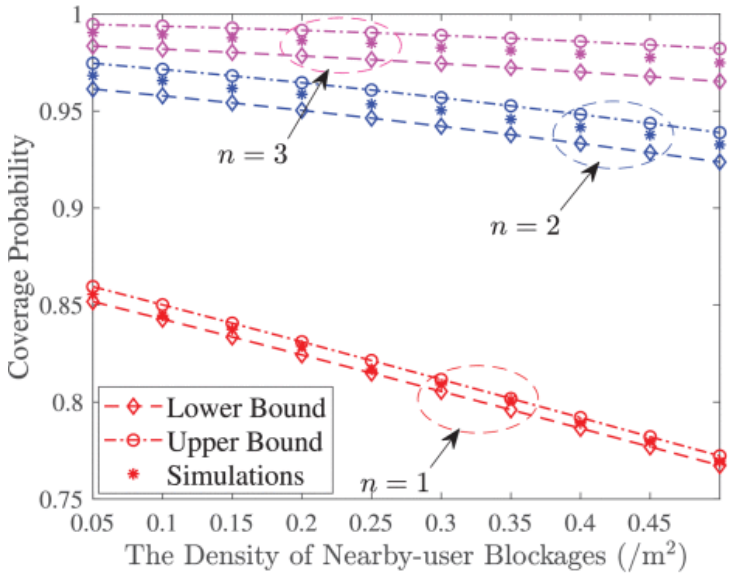


(a) $R_{\mathrm{b}} = 50$ m

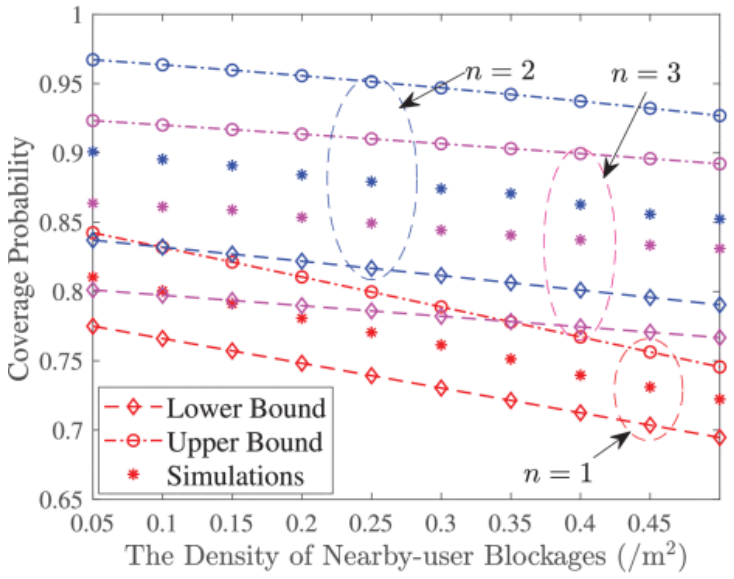


(b) $R_{\mathrm{b}} = 250$ m

Fig. 11. With different distance between the BS and the UE, the coverage probability to the density of nearby-user blockages.

In Fig. 12, the impact of SNR threshold on the coverage probability is illustrated. When the SNR threshold is relatively low, e.g., below 20 dB, small-size RISs can provide enough received signal power gain to meet the SNR threshold. Hence, the coverage probability is mainly affected by blockages. In other words, the blockage probability is dominant in the impact on the coverage probability. Therefore, large $n$ is preferable when SNR threshold is low, e.g., inFig. 12 (b), $n = 4$ has the highest coverage probability when the SNR threshold $T = 15$ dB. However, as the SNR threshold rises, only large-size RISs can provide enough received signal power gain to meet the SNR threshold. In other words, the received signal power gain becomes dominant in the coverage probability. Accordingly, small $n$ is more suitable for the networks with high SNR threshold, e.g., $n = 1$ leads to the highest coverage when $T = 25$ dB.

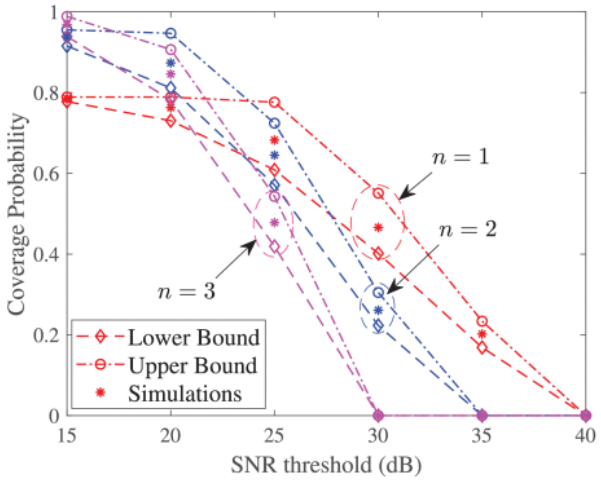


(a) With different $n$, the coverage probability to SNR threshold

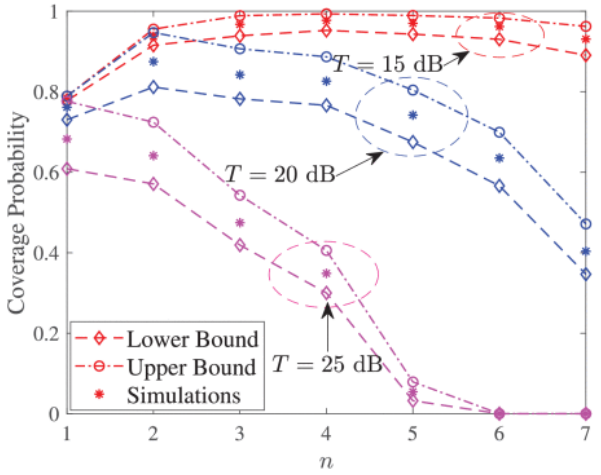


(b) With different SNR threshold, the coverage probability to $n$

Fig. 12. The coverage probability to SNR threshold and to $n$.

In Fig. 13, the coverage probabilities of RIS-assisted network when RISs are much closer to the UE than the BS are shown. The analytical results match with simulations well, and small gaps exist because of the approximation in which the horizontal distance between the BS and connected RIS is equal to the horizontal distance between the BS and UE. In bothFig. 13 (a) and (b), $n = 2$ leads to the highest coverage probability except when building blockage density rises to around $2.7 \times 10^{-3} / \mathrm{m}^2$. In addition, as blockage density increases, coverage with low value of $n$ drops faster than coverage with high value of $n$ .Fig. 13further demonstrates that densely deployed small-scale RISs outperform sparsely deployed large-scale RISs in scenarios with dense blockages in terms of coverage enhancement.

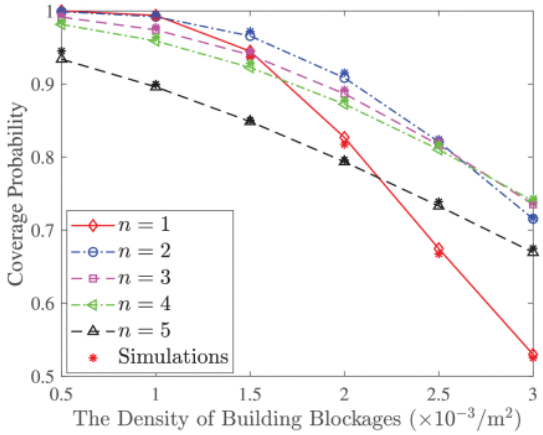


(a) With different $n$, the coverage probability to the density of building blockages

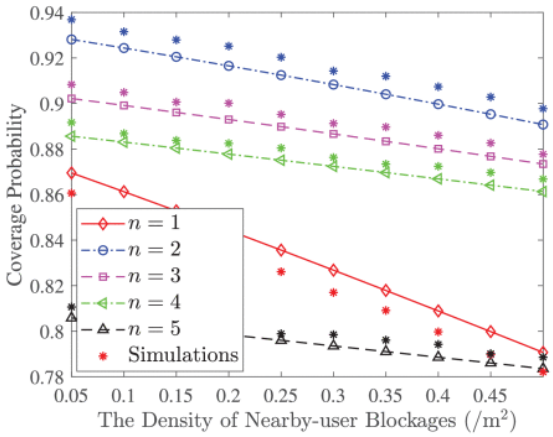


(b) With different $n$, the coverage probability to the density of nearby-user blockages

Fig. 13. The coverage probability when RISs are much closer to the UE than the BS.

In Fig. 14, the function of coverage probability to cost is illustrated. Fig. 14 (a)shows that the coverage probability and the cost increase as the number of RISs grows. Particularly, with the same amount of cost increase, higher building density causes larger growth of coverage probability. Fig. 14 (b)indicates the impact of the cost exponent on the coverage probability. The results show that high value of cost exponent leads to low cost effectiveness of densely deployed small-scale RISs, e.g., even in the environment with densely deployed blockages, when ς=0.75, 60% cost growth causes only 40% coverage enhancement. Therefore, lower cost exponent leads to higher cost effectiveness when densely deployed small-scale RISs are deployed, while higher cost exponent causes higher cost effectiveness when sparsely deployed large-scale RISs are deployed.

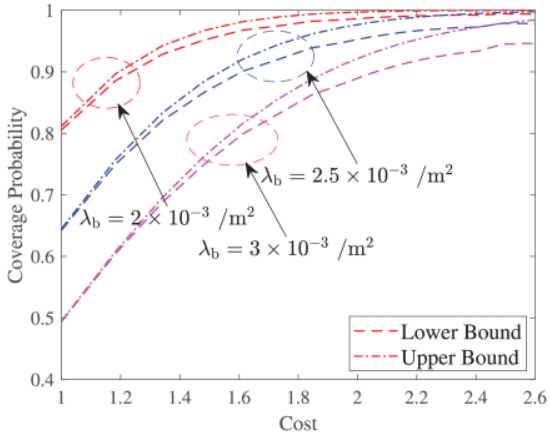


(a) With different building density $\lambda_b$, the coverage probability to cost. $\varsigma = 0.5$.

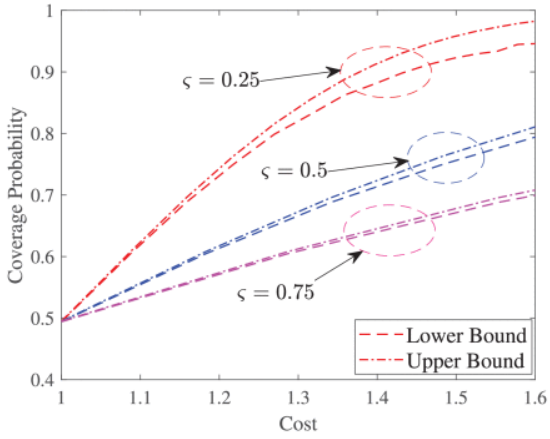


(b) With different cost exponent $\varsigma$, the coverage probability to cost. $\lambda_b = 3 \times 10^{-3}$ /m$^2$.

Fig. 14. Cost effectiveness: the function of coverage probability to cost with different cost exponent $\varsigma$.

$$R_b = 50m$$

*Summary of Insights:*According to the analysis of numerical results, the main insights are summarized as follows:

The balance between RIS density and RIS size is also the tradeoff between blockage probability and path loss.

Blockage density has more impact on coverage probability when sparsely deployed large-scale RISs are deployed, while transmission distance has more impact on coverage probability when densely deployed small-scale RISs are deployed.

In the same cell of a BS, small-scale RISs are preferable to be deployed around the cell center to decrease blockage probability, while large-scale RISs are preferable to be deployed in the cell edge to decrease blockage probability and compensate path loss.

Densely deployed small-scale RISs are better option when SNR threshold is relatively low, while sparsely deployed large-scale RISs win when SNR threshold is relatively high.

Cost effectiveness of densely deployed small-scale RISs depends on how the number of RISs affects the network cost. If the cost grows linearly with the number of RISs, densely deployed small-scale RISs are not cost-effective even in the environment with densely deployed blockages.

# 5. Conclusion

In this report, analytical results for RIS deployment strategy analysis considering both building blockages and human blockages have been provided. The proposed tractable upper and lower bounds of coverage probability closely match the trend of simulations, demonstrating their usefulness in replacing time-consuming simulation in RIS deployments. Moreover, the impact of building density, nearby-user density, transmission distance and SNR threshold on RIS-assisted mmWave network coverage was analyzed, respectively. The results showed that as the number of RISs grows, if the increase of network cost is below the linear increase at certain level, more small RISs are better option for high building blockage density and/or short transmission distance, e.g., urban area, whereas fewer large RISs are more suitable for low building blockage density and/or long transmission distance, e.g., rural area. In addition, if the network cost grows linearly with the number of RISs, densely deployed small-scale RISs are not a cost-effective option even in the environment with densely deployed blockages. Our works can be used as a guidance for practical RIS deployment in built environments where blockages are common.

# References


i. J. G. Andrews et al., "What will 5G be? " IEEE J. Sel. Areas Commun., vol.32, no. 6, pp. 1065-1082, Jun.2014.

2. Z. Li, H. Hu, J. Zhang，and J. Zhang, "Enhancing indoor mmWave wireless coverage: Small-cell densification or reconfigurable intelligent surfaces deployment?" IEEE Wireless Commun. Lett.，vol. 10, no. 11, pp.2547-2551，Nov.2021.
3. Q. Wu and R. Zhang, "Towards smart and reconfigurable environment: Intelligent reflecting surface aided wireless network," IEEE Commun. Mag.，vol.58, no. 1, pp. 106-112, Jan.2020.
4. C. Huang et al., "Holographic MIMO surfaces for 6G wireless networks: Opportunities, challenges, and trends," IEEE Wireless Commun.，vol. 27, no. 5, pp. 118-125, Oct.2020.
5. E. Basar，M. Di Renzo，J. De Rosny，M. Debbah，M. Alouini, and R. Zhang, "Wireless communications through reconfigurable intelligent surfaces," IEEE Access，vol. 7, pp. 116753-116773,2019.
6. Y. Zhu，M. Li, Y. Liu, Q. Liu, Z. Chang, and Y. Hu, "DRL-based joint beamforming and BS-RIS-UE association design for RIS-assisted mmWave networks,"2022, arXiv:2202.09524.
7. C. Huang et al., "Multi-hop RIS-empowered terahertz. communications: A DRL-based hybrid beamforming design," IEEE J. Sel. Areas Com-mun.，vol.39, no. 6, pp. 1663-1677, Jun.2021.
8. W. Xu, J. An, C. Huang, L. Gan, and C. Yuen，"Deep reinforcement learning based on location-aware imitation environment for RIS-aided mmWave MIMO systems," IEEE Wireless Commun. Lett., vol. 11, no.7, pp. 1493-1497, Jul. 2022.

9. L. Wei, C. Huang，G.C. Alexandropoulos，C. Yuen，Z. Zhang，and M. Debbah, "Channel estimation for RIS-empowered multi-user MISO wireless communications," IEEE Trans. Commun.，vol. 69, no. 6, pp.4144-4157, Mar. 2021.
10. T. Van Chien, L. T. Tu, S. Chatzinotas，and B. Ottersten，"Coverage probability and ergodic capacity of intelligent reflecting surface-enhanced communication systems, IEEE Commun. Lett., vol.25, no. 1, pp.69-73, Jan. 2021.
11. L. Yang， Y. Yang，D. B. D. Costa，and I. Trigui, "Outage probability and capacity scaling law of multiple RIS-aided networks," IEEE Wireless Commun. Lett.， vol. 10, no.2, Pp. 256-260, Feb.2021.
12. Y. Zhang, J. Zhang, M. D. Renzo，H. Xiao，and B. Ai, "Performance analysis of RIS-aided systems with practical phase shift and amplitude response," IEEE Trans. Veh. Technol.，vol. 70, no. 5，pp. 4501-4511, May 2021.
13. Papazafeiropoulos, C. Pan, A. Elbir, P. Kourtessis, S. Chatzinotas, and J. M. Senior, "Coverage probability of distributed IRS systems under spatially correlated channels," IEEE Wireless Commun. Lett.，vol. 10, no. 8, pp. 1722-1726, Aug.2021.
14. T. Van Chien, A. K. Papazafeiropoulos, L. T. Tu, R. Chopra, S. Chatzinotas，and B. Ottersten, "Outage probability analysis of IRS-assisted systems under spatially correlated channels," IEEE Wireless Commun. Lett.，vol. 10, no.8, pp. 1815-1819, Aug.2021.
15. Q. Tao，J. Wang，and C. Zhong, "Performance analysis of intelligent reflecting surface aided communication systems," IEEE Commun. Lett., vol.24, no. 11, pp.2464-2468，Nov.2020.
16. M. Salhab and M. H. Samuh, "Accurate performance analysis of reconfigurable intelligent surfaces over Rician fading channels," IEEE Wireless Commun. Lett.， vol.10, no. 5, pp. 1051-1055, May 2021.
17. J.G. Andrews, F. Baccelli,and R. K. Ganti, "A tractable approach to coverage and rate in cellular networks," IEEE Trans. Commun.，vol.59,no.11, pp.3122-3134，Nov.2011.
18. J. Lyu and R. Zhang, "Spatial throughput characterization for intelligent reflecting surface aided multiuser system," IEEE Wireless Commun. Lett.， vol. 9, no. 6, pp.834-838, Jun. 2020.
19. J. Ye, A. Kammoun, and M.-S. Alouini, "Spatially-distributed RISs vs relay-assisted systems: A fair comparison," IEEE Open J. Commun. Soc.,vol. 2, pp.799_817,2021.
20. M. Nemati, J. Park, and J. Choi, "RIS-assisted coverage enhancement in millimeter-wave cellular networks," IEEE Access, vol. 8, pp.188171-188185，2020.
21. Y. Zhu, G. Zheng, and K.-K. Wong, "Stochastic geometry analysis of large intelligent surface-assisted millimeter wave networks," IEEE J. Sel. Areas Commun.，vol.38, no.8, pp. 1749-1762, Aug.2020.
22. J. Lyu and R. Zhang," Hybrid active/passive wireless network aided by intelligent reflecting surface: System modeling and performance analysis," IEEE Trans. Wireless Commun. vol.20, no. i1, pp.7196-7212, Nov. 2021.
23. T. Shafique, H. Tabassum, and E. Hossain, "Stochastic geometry analysis of IRS-assisted downlink cellular networks," IEEE Trans. Commun., vol.70, no.2, Pp. 1442-1456, Feb.2022.
24. M. Di Renzo and J. Song, "Reflection probability in wireless networks with metasurface-coated environmental objects: An approach based on random spatial processes," EURASIP J. Wireless Commun. Netw., vol.2019, no. 1, p. 99, Apr. 2019.
25. C. Psomas, H. A. Suraweera，and I. Krikidis， "On the association with intelligent reflecting surfaces in spatially random networks," in Proc. IEEE Int. Conf. Commun. (ICC)，Montreal，QC，Canada，Jun.2021, pp. 1-6.

26. Y. Chen, B. Zhang, M. Ding, D. Lopez-Perez, and H. Zheng, "Performance analysis of wireless networks with intelligent reflecting surfaces," in Proc. IEEE Wireless Commun. Netw.Conf. (WCNC), Nanjing, China, Mar. 2021, pp. 1-6.
27. M.A. Kishk and M.-S. Alouini,"Exploiting randomly located blockages for large-scale deployment of intelligent surfaces," IEEE J. Sel. Areas Commun.， vol.39, no. 4, pp. 1043-1056, Apr. 2021.
28. W. Tang et al., "Wireless communications with reconfigurable intelligent surface: Path loss modeling and experimental measurement," IEEE Trans. Wireless Commun.，vol. 20, no.1, pp. 421-439, Jan. 2021.
29. Thornburg, T. Bai, and R. W. Heath, Jr. "Performance analysis of outdoor mmWave ad hoc networks," IEEE Trans. Signal Process., vol.64, no. 15, Pp. 4065-4079, Aug. 2016.
30. Y. Zhu, L. Wang, K. K. Wong, and R.W. Heath, Jr.，"Secure communications in millimeter wave ad hoc networks," IEEE Trans. Wireless Commun.，vol.16, no. 5, pp.3205-3217, May 2017.
31. T. Bai, R. Vaze, and R. W. Heath, Jr., "Analysis of blockage effects on urban cellular networks," IEEE Trans. Wireless Commun., vol.13, no. 9, pp.5070-5083, Jun. 2014.
32. P. Liu and A. Springer, "Space shift keying for LOS communication at mmWave frequencies," IEEE Wireless Commun. Lett.，vol. 4, no. 2, pp. 121-124，Apr. 2015.
33. Y.Z hang, J. Zhang, X. Chu, and J. Zhang, "Lower-bound capacity-based wireless friendliness evaluation for walls as reflectors," IEEE Trans. Broadcast.，vol.67, no. 4, pp. 917-924, Dec.2021.
34. E. Bjornson，J. Hoydis, and L. Sanguinetti, "Massive MIMO networks: Spectral, energy and hardware efficiency," Found. Trends Signal Process.，vol.11, nos.3-4, pp. 154-655，Nov. 2017.
35. E. Bjornson and L. Sanguinetti, "Rayleigh fading modeling and channel hardening for reconfigurable intelligent surfaces," IEEE Wireless Com-mun. Lett.， vol.10, no. 4, pp.830-834，Apr. 2021.
36. T.S. Rappaport et al., "Millimeter wave mobile communications for 5G cellular: It will work!" IEEE Access，vol. 1, pp. 335-349,2013.
37. M. Gapeyenko et al. "Analysis of human-body blockage in urban millimeter-wave cellular communications, in Proc. IEEE Int. Conf. Commun. (ICC), May 2016, Pp. 1-7.
38. X. Yang et al.，"Design and implementation of a TDD-based 128 antenna massive MIMO prototype system, "China Commun.，vol. 14, no. 12, pp. 162-187,2017.